Continuous Bed Motion Vs. Step-and-Shoot Acquisition on Clinical Whole-Body Dynamic and Parametric PET Imaging

Nicolas A. Karakatsanis[1], *Member, IEEE*, Valentina Garibotto[1], Olivier Rager[1] and Habib Zaidi[1,2,3], *Senior Member, IEEE*

***Abstract* – Continuous bed motion (CBM) has been recently introduced in the clinic as an alternative PET acquisition mode with respect to the traditional time-discretized step-and-shoot (SS) multi-bed acquisitions. In CBM mode, each slice can be considered as a different bed, since it is scanned over a different acquisition window. By reducing scan time discretization from a whole bed down to a single slice, the CBM acquisition offers additional degrees of freedom when designing acquisition protocols and thus larger margins for their optimization. Therefore, CBM mode could be particularly important for protocols of higher complexity, such as whole-body (WB) dynamic PET acquisitions. However, only a few studies have quantitatively validated the 2 modes on clinical data. In this work, we evaluate CBM vs. SS quantitative performance on a set of clinical data acquired over a 0-60min period using a WB dynamic PET acquisition protocol with a Biograph mCT TOF scanner. The TOF resolution (580ps) of the scanner allowed selecting faster CBM speeds (4.2mm/sec) and equivalent SS frames (30sec/bed), eventually permitting acquisition of 12 WB total passes of which half were performed in CBM mode and half in SS mode. The two modes were alternated between successive passes to allow a balanced interleaving of post-injection time between them to ensure an objective comparison. The evaluation of the 2 modes in terms of target-to-background (TBR) contrast and contrast-to-noise ratio (CNR) has been conducted for various noise levels by gradually adding all respective passes from each mode as well as in the parametric images after applying post-reconstruction WB Patlak analysis. Our results indicate a bias of ~10% between the 2 modes for the low count frames, reducing to <3% as we gradually add all respective frames. In addition, a small bias of <10% was observed in Patlak images at overlapped slices between beds, which is attributed to the non-uniformity of the axial sensitivity profile of SS mode.**

I. Introduction

The limited axial field-of-view (FOV) of modern clinical PET scanners, also denoted as bed position FOV, has led to multi-bed acquisitions by translating the bed table axially at multiple positions in order to allow for whole-body (WB) imaging. Currently, most PET scanners operate in step-and-shoot (SS) acquisition mode, involving sequential scans over multiple stationary bed positions, by employing a step-wise bed motion [1-4]. This mode simplifies data acquisition synchronization with time and position, as the gantry bed remains stationary at fixed bed positions during the acquisition.

However, due to the stationary axial position of the scanner FOV during 3-dimensional (3D) PET acquisition, the slices close to the two edges of the axial FOV are always intercepted by smaller number of coincidence lines of response (LORs), compared to the central slices, thus leading to a significantly lower 3D PET sensitivity at the axial edges of each bed position FOV [5-7]. In order to sufficiently compensate for the lower sensitivity at the edge relative to the central slices of each bed position, scan overlapping between subsequent bed position FOVs is currently applied in the clinic as a straightforward, yet satisfactory solution [8-11]. However, the uniformity in axial sensitivity and noise may not be always adequately restored with scan overlapping, especially when shorter scan time frames per bed position are utilized or low uptake regions are targeted. In these cases, noise levels at the edge slices of each bed position FOV may be considerably high, thus potentially leading to quantification errors in the final reconstructed PET images [12,13].

In addition, with the advent of new technologies, such as Time-of-Flight (TOF) and model-based resolution recovery reconstruction [14-16], the scan time per bed can be reduced enabling (i) faster WB PET scans for the same noise-equivalent count rate (NECR) as well as (ii) clinically feasible WB dynamic PET acquisitions for enhanced quantification [17-20]. However, SS bed motion and the associated bed inertia may become more apparent with shorter bed frames, thus causing potential patient discomfort. Moreover, in the case of WB dynamic protocols a significantly higher number of bed transitions could be required, thus further compromising patient comfort and jeopardizing clinical feasibility [12]. Furthermore, the extent of the FOV in multi-bed SS PET acquisitions is constrained to an integer number of beds, thus considerably limiting the optimization of clinical multi-bed PET scan protocols.

On the other hand, the concept of PET scanners supporting continuous bed motion (CBM) technology has also been proposed in the past and tested as a prototype on modified PET scanners [21-29]. Recently, CBM acquisition and reconstruction features have also been integrated in the clinical commercial PET/CT system of Biograph mCT by Siemens Molecular Imaging, as an alternative acquisition

This work was supported by the Swiss National Science Foundation under Grant SNSF 31003A-149957.

[1] N. A. Karakatsanis (e-mail: nikolaos.karakatsanis@unige.ch), V. Garibotto, O. Rager and H. Zaidi are with the Division of Nuclear Medicine and Molecular Imaging, School of Medicine, University of Geneva, Geneva, Switzerland

[2] H. Zaidi is also with Geneva Neuroscience Centre, University of Geneva, Geneva, Switzerland

[3] H. Zaidi is also with the Department of Nuclear Medicine and Molecular Imaging, University of Groningen, Groningen, Netherlands

978-1-4673-9862-6/15/$31.00 ©2015 IEEE

mode [30-34]. Contrary to the traditional time-discretized SS multi-bed acquisitions, the bed gantry in CBM mode moves continuously over all transaxial slices while acquiring data [34]. Effectively, each slice can be now considered as a different bed position, since it is scanned over a different time acquisition window or frame. By reducing scan time discretization from a whole bed position down to a single transaxial slice, CBM acquisitions can offer additional degrees of freedom and thus larger margins of optimization when designing acquisition protocols of extended or WB FOVs. These benefits could considerably increase for dynamic PET protocols of extended axial FOVs, as they involve multiple passes [12]. Currently, only a few studies have quantitatively validated the two modes [34-36]. They have been limited to single-pass WB clinical studies, where comparison objectiveness can be compromised as the complete dataset from each mode must be acquired separately, leading to ~15-20min time shifts of the acquisition window between SS and CBM data.

In this study, we quantitatively investigate the novel clinical application of CBM vs. SS acquisitions for our proposed WB dynamic PET scan protocol [12]. Furthermore, a WB parametric imaging framework has been developed capable of utilizing time information from the dynamic CBM WB PET data. For that purpose, a previously proposed post-reconstruction statistical regression framework has been adapted from a bed-by-bed to a more finely sampled slice-by-slice temporal data graphical analysis [13]. In addition, we exploit the convenience of multiple dynamic WB scan protocols to alternately perform short SS and CBM WB passes in order to uniquely acquire a more uniform and time-balanced dataset that would allow less time-dependent and, thus, more objective comparative clinical evaluations between the two scan modes.

II. Methods and Materials

A. Continuous bed motion vs. step-and-shoot acquisition mode

In CBM mode, each transaxial slice, here denoted simply as a slice, of the imaging subject can be scanned at all possible axial positions of the scanner FOV as the gantry bed continuously moves across all slices and along the axial direction [34]. As a result, the scanner sensitivity profile can be uniform across any subset of axial FOV slices for which the bed speed remains constant, except from the axial slices close to the two edges of the entire WB imaging FOV (Fig. 1c). In addition, in the case of a constant bed speed, the time-sensitivity profile, i.e. the number of counts vs. scan time, for each slice is also identical. Therefore, the blue area under the curves (AUCs) in Fig. 1d, that quantify the total number of counts or sensitivity, remains the same for all slices, except those close to the 2 edges of the WB FOV (not shown here).

On the contrary, with SS mode the axial sensitivity drops at the two edges of each bed position, not just at the 2 edges of the entire WB FOV and, thus, overlapping is necessary to restore sensitivity (Fig. 1a), though noise may still remain relatively higher for the overlapped slices. As the bed remains stationary at each axial position during acquisition, the time-sensitivity profile is characterized by a rectangular shape of a constant number of counts (Fig. 1b). However, the height of the profile, i.e. the number of counts or sensitivity, may vary considerably between the central and edge slices of each bed position (not shown here).

In Fig. 1 we assumed a uniform source distribution across the axial dimension and studied the respective axial sensitivity distribution if the motion speed of the bed remains constant. However, in reality the activity source distribution in a human WB PET scan may vary considerably along the axial direction depending primarily on the tracer kinetics, the amount of administered tracer dosage and the patient body type. As a result, the relative composition of prompt counts in trues, randoms and scatter may also be affected significantly, causing significant variations, between adjacent beds or even axial slices, in the noise equivalent count rate (NECR) of the raw projection data and the signal-to-noise ratio (SNR) of the results [37,38]. If this effect is not taken into account, the WB images may suffer from significant noise fluctuation between the slices, potentially degrading lesion detectability and quantitative evaluations. Previously, various optimization strategies had been proposed to regulate both the administered amount of tracer dosage and the scan time per bed position in SS acquisition modes in an attempt to achieve a maximal and at the same time uniform average NECR performance across all beds of the WB FOV [39-44]. However, these approaches are not sufficient to compensate for any sensitivity non-uniformities between adjacent slices of the same bed, due to the inherent limitations of SS acquisition modes.

Nevertheless, CBM mode offers the unique capability to further improve axial uniformity in the sensitivity profile by adjusting the axial bed speed profile over different subset of slices. This type of acquisition protocol optimization can be driven by a noise-related quantitative criterion such that a a-priori noise-equivalent count rate (NECR) axial distribution or other CT-guided estimates of emission data noise. The information from the CT or MRI scan on hybrid PET/CT or PET/MR acquisition protocols could allow a rough yet sufficient approximation of the noise estimates on a slice-by-slice basis. Then, the gantry bed/table could be programmed to move faster across any particular set of slices associated with overall higher NECR scores and slower over the rest of the slices of the WB imaging FOV. Thus, with CBM technology a higher degree of noise uniformity may be achieved across the entire axial FOV of a WB PET scan.

In addition, unlike SS mode where all non-overlapped slices of every bed are simultaneously acquired at the same time window (Fig. 1b), in CBM mode any 2 successive slices are scanned in temporally shifted acquisition time windows (Fig. 1d). As a result, in CBM scans a unique time stamp should be assigned not to the data of the entire bed position, as was the case with SS mode, but to the data of each slice.

Furthermore, CBM allows for more flexible sizes of the extended axial FOV in terms of integer number of slices, as opposed to integer number of beds, thus replacing the concept of multi-bed imaging in SS acquisitions with that of "multi-slice" imaging in CBM mode. Furthermore, after completion of a CBM acquisition, any shifted limited axial FOV position

within the extended FOV can be selected to retrieve the raw data, bin the corresponding sinogram and reconstruct the images at the particular axial location. Thus, unlike SS mode where bed positions are fixed, CBM allows for customized 3D PET reconstructions directly from user-defined bed FOV positions. This CBM feature could be further exploited to synthesize a dynamic set of 3D sinograms corresponding to overlapped axial FOVs between different dynamic extended CBM acquisitions of the same patient. Thus, a direct 4D reconstruction from different dynamic CBM scans of the same subject could become possible, provided a common axial FOV overlap exists between the CBM passes. Previously proposed conventional direct 4D WB parametric reconstruction algorithms [45-49] could be accordingly modified for that purpose.

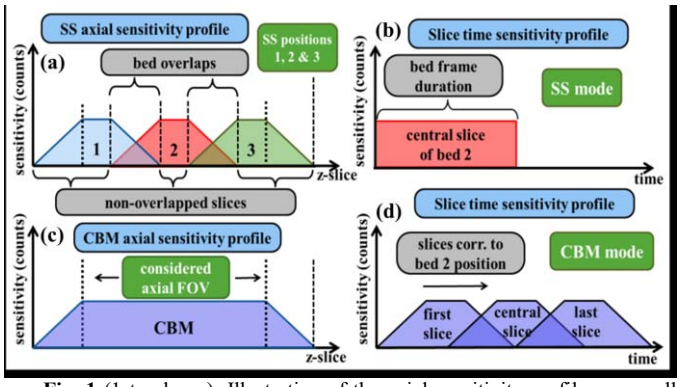

Fig. 1 (1st column): Illustration of the axial sensitivity profile across all slices of an extended axial FOV for (a) SS and (c) CBM modes. (2nd column): Sensitivity profile of particular axial FOV slices vs. scan time for (b) a central slice with SS mode and (d) central and the two edge slices with CBM mode of a slices set corresponding to bed position 2. The two edge slices at (d) are denoted as "first" and "last", according to the time order with which they were scanned.

B. Utilization of time information of dynamic WB CBM PET data

One of the major differences between SS and CBM mode is their different synchronization schemes between data acquisition and scan time. In SS mode, all non-overlapped bed slices are acquired at the same time window, while a weighted average time is assigned for the overlapped slices [1-4]. On the contrary, in CBM mode each slice has been scanned at a unique average time relative to injection, accurately determined by the slice axial position and the bed speed profile [34].

As a result, if we assume similar kinetics across a certain region extending over a few neighboring slices, with CBM mode we could, unlike SS case, potentially acquire multiple time samples of that region's time activity curve (TAC) at every single frame by utilizing measurements from voxels of the same region but across a group of neighboring slices of that frame. This capability is demonstrated in Fig. 2 for bed frame 3 of an early pass (pass #1) where the activity is expected to change relatively faster and thus a higher temporal frequency could be useful. The top chart demonstrates the time flow of the dynamic WB acquisition protocol, while the two charts at the bottom present the detailed scan time flow for all 109 slices of bed 3 from pass 1 to illustrate the potential differences in temporal sampling rates between CBM (left) and SS (right) acquisition modes, assuming the same TAC for a few neighboring slices.

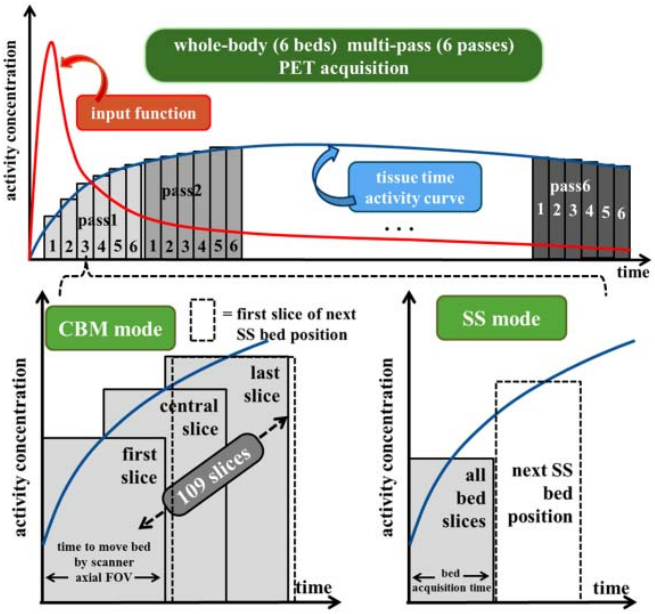

Fig. 2 (1st row): Simulated example of dynamic WB PET acquisition time flow chart of a hypothetical input function and region TAC extending over all dynamic WB passes. (2nd row): Detailed chart of activity vs. scan time for all 109 slices of bed 3 from WB pass 1, for CBM (left) and SS (right) mode. In CBM mode, each slice is scanned at a different time window, resulting in potentially higher number of temporal samples for the input function and regional TACs, assuming the same TAC for a set of adjacent slices. In SS mode, all bed slices are scanned simultaneously at a stationary bed position, thus only one temporal sample can be obtained.

C. Alternating SS and CBM dynamic WB acquisition PET protocol

In this work, we performed a comparative evaluation of CBM vs. SS quantitative performance on a set of clinical FDG PET data using a WB dynamic protocol on a Siemens Biograph mCT Flow TOF scanner with both SS and CBM capabilities [16,34]. The higher sensitivity achieved with the mCT TOF resolution of 580ps [16] allowed for faster constant bed motion (4.2mm/sec) and count-equivalent SS frames (30sec/bed) [34], thus permitting acquisition of 12 WB (6 beds) passes (10-60min p.i.), of which half were performed in SS, including the first pass, and half in CBM mode, by alternating the two modes successively to allow a balanced interleaving of time between them (Fig. 3).

Both types of WB passes were completed at the same time and according to our previously proposed WB dynamic PET acquisition protocol adapted for the mCT TOF PET scanner. The utilization of fast (~3min each) and alternating SS and CBM WB passes is expected to minimize any major temporal effects between successive passes, due to physiological uptake variations, and enable objective comparisons between SS and CBM modes from a single clinical scan.

The comparative evaluation was performed on both static SUV PET and parametric WB images. In particular, the data from the last 3 dynamic WB passes of each scan mode, when FDG TACs are expected to be less time-variable, were added to synthesize PET images of lower noise. The specific set of frames was selected, as FDG TACs are expected to be less time-variable during that period and with higher uptake at the regions of interest. Besides, that period corresponded to post 60min time windows, thus better matching with the standard SUV acquisition window for FDG PET scans.

In addition, WB tracer uptake rate (K_i) images were produced by employing standard and generalized Patlak analysis (sPatlak & gPatlak) [50-53]. In order to further minimize the acquisition time window effect on WB K_i images, as observed in a previous study [54], Patlak analysis was applied on 3 different sets of passes, that were selected such that they correspond to time windows of equal duration and with a minimal time shift between them: (i) the first 5 SS frames (SS passes 1-5), (ii) the first 5 CBM frames (CBM passes 1-5) and (iii) the last 5 SS frames (SS passes 2-6).

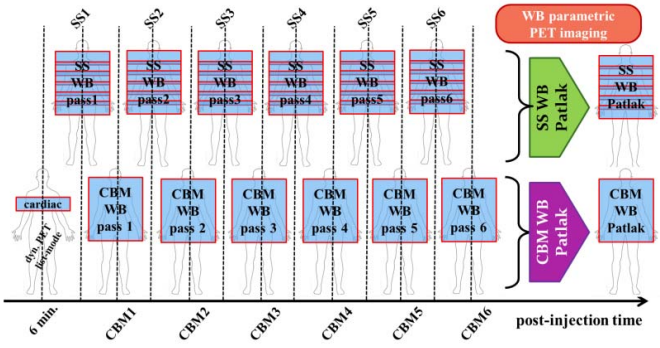

Fig. 3 Dynamic WB PET protocol with alternating scheme between SS (first) and CBM passes and generation of WB Patlak images from the two datasets.

III. Results and Discussion

The qualitative comparison of the reconstructed clinical images in Figs. 4 and 5 suggest relatively small overall difference or bias (~10%) between SS and CBM modes for the last dynamic passes, reducing to <3% as we add the last 3 respective frames. Thus, we observe overall small differences that tend to become negligible at lower noise levels.

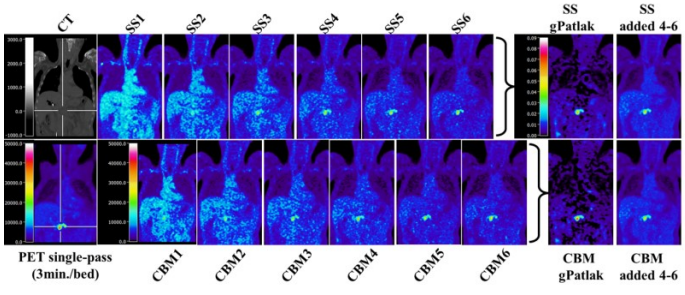

Fig. 4 Qualitative evaluation of (1st row) SS vs. (2nd row) CBM WB dynamic PET and of gPatlak K_i clinical images. Comparisons with CT and SUV images.

In addition, our quantitative results in (s/g)Patlak WB images for the 2 displayed neighboring high uptake regions located at a bed overlap (Fig. 5) indicate a difference of less than 10% in target-to-background (TBR) contrast and contrast-to-noise ratio (CNRs) scores between the 3 evaluated time windows (Fig. 6).

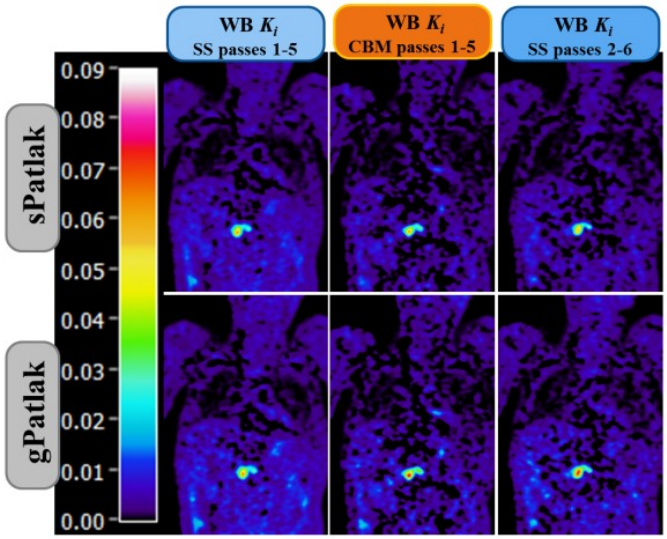

Fig. 5 Qualitative evaluation of WB (1st row) sPatlak and gPatlak (2nd row) *Ki* images when 3 different 5-pass sets are employed.

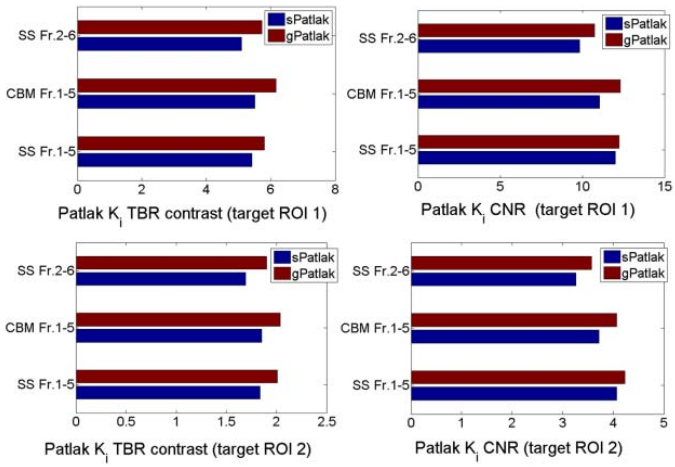

Fig. 6 TBR and CNR quantitative analysis over the 2 neighboring high K_i target regions displayed in Fig. 5.

Moreover, K_i TBR and CNR scores were systematically reduced at the latest time window (SS Frames 2-6) for both Patlak methods but with larger reduction in the case of sPatlak, suggesting that the differences can be partially attributed to the previously observed underestimation of K_i TBR and CNR at later windows, especially in the case of sPatlak images due to lack of modeling of FDG uptake reversibility [52-54]. Furthermore, very small TBR and CNR differences were found between the two earliest time windows (SS frames 1-5 vs. CBM frames 1-5), compared to the respective differences between the latest 2 windows (CBM frames 1-5 vs. SS frames 2-6). By taking into account that TBR and CNR are expected to be underestimated linearly with

the shift of the acquisition time windows to later periods, the previous non-linear decrease of TBR and CNR metrics could be attributed to TBR and CNR enhancements for CBM mode, compared to SS. In addition, the measured differences correspond to a high uptake region situated over a range of overlapped slices, where the differences between SS and CBM mode are expected to be particularly observed. Finally, generalized Patlak was less sensitive to both the choice of acquisition mode and time window, thus demonstrating a higher quantitative value.

IV. Conclusions And Future Studies

In this study, we successfully utilized the unique properties of a validated dynamic WB PET acquisition protocol to objectively compare the performance of SS and CBM acquisition modes on a single patient scan both on SUV and Patlak K_i images. The temporal and balanced interleaving of the two scan modes between successive WB passes of the same dynamic WB scan minimized any non-negligible temporal effects that could hamper the objective evaluation of the quantitative TBR and CNR metrics. Moreover, a post-reconstruction generalized Patlak analysis framework was developed to properly handle the novel time-sensitivity profiles of CBM acquisitions.

Furthermore, the quantitative analysis on dynamic PET images for a high uptake region located at an overlapped region between two successive beds, demonstrated an enhanced TBR and CNR performance for the CBM mode but with differences becoming negligible at lower noise levels. Similar analysis on (s/g)Patlak Ki images suggested the same superiority for CBM mode, but with more apparent differences in the case of sPatlak method. Overall, our results suggest applying CBM over SS acquisitions, when possible and demonstrated the clinical feasibility and benefits of WB dynamic CBM acquisitions and parametric imaging analysis.

In the future, we plan to expand the validation methods to more patients and further investigate the effects of dynamic WB CBM acquisition in direct 4D WB parametric reconstruction algorithms and in combination with methods to synthesize SUV from 4D PET data [55] and infer early input function measurements from population-based methods [56,57].

V. Acknowledgments

The authors would like to gratefully acknowledge support by the Swiss National Science Foundation under Grant SNSF 31003A-149957.

References

[1] S. F. Schubert, S. Pajevic and R. E. Carson “Whole body PET using overlapped 3D acquisition and weighted image summation,” IEEE Nucl Sc Symp Med Imag Conf (NSS/MIC), Anaheim, CA, p. 1285-1289, 1996

[2] M. Dahlbom, P.D. Cutler, W.M. Digby, W.K. Luk, and J. Reed, “Characterization of sampling schemes for whole body PET imaging,” IEEE Trans Nucl Sc, 41, p. 1571-1576, 1994

[3] P.D. Cutler and M. Xu, ”Strategies to improve 3D whole-body PET image reconstruction,” Phys Med Biol, 41, p. 1453-1467, 1996

[4] A. Chatziioannou and M. Dahlbom, "Study of the effects of whole body PET spatial sampling schemes on data SNR," IEEE Nucl Sc Symp Med Imag Conf (NSS/MIC), Anaheim, CA, p. 1295-1299, 1996

[5] S. R. Cherry, M. Dahlbom and E. J. Hoffman, “3D PET using a conventional multislice tomograph without septa,” J Comp Assist Tomogr, 15(4), p. 655-668, 1991

[6] D. W. Townsend, A. Geissbühler, M. Defrise, E. J. Hoffman, T. J. Spinks, D. L. Bailey, M. C. Gilardi, and T. Jones, "Fully three dimensional reconstruction for a PET camera with retractable septa," IEEE Trans Med Imag, MI-10, p. 505-512, 1991

[7] S. Pajevic, M.E. Daube-Witherspoon, S.L. Bacharach, and R.E. Carson, ”Noise characteristics of 3D and 2D PET images,” IEEE Trans Med Imag, 17(1), p. 9-23, 1998

[8] P.E. Kinahan and J.G. Rogers, “Analytic three dimensional image reconstruction using all detected events,” IEEE Trans Nucl Sci, 36, p. 964-968, 1989

[9] S.R. Cherry, M. Dahlbom, and E.J. Hoffman, “Evaluation of a 3D reconstruction algorithm for multi-slice PET scanners,” Phys Med Biol, 37, p. 779-790, 1992

[10] P.E. Kinahan and J.S. Kairp, “Figures of merit for comparing reconstruction algorithms with a volume imaging PET scanner,” Phys Med Biol, 39, p. 63 1-642, 1994

[11] T.K. Lewellen, S.G. Kohlrriyer,R.S. Miyaoka, M.S. Kaplan, C.W. Steams, and S.E Schubert, “Investigation of the performance of the General Electric Advance positron emission tomograph in 3D mode,” IEEE Trans Nucl Sci, 43, p. 2199-2206, 1996

[12] N. A. Karakatsanis, M. A. Lodge, A. K. Tahari, Y. Zhou, R. L. Wahl and A. Rahmim, “Dynamic whole-body PET parametric imaging: I. Concept, acquisition protocol optimization and clinical application,” Phys Med Biol, 58(20), p. 7391-7418, 2013

[13] N. A. Karakatsanis, M. A. Lodge, Y. Zhou, R. L. Wahl and A. Rahmim, “Dynamic whole-body PET parametric imaging: II. Task-oriented statistical estimation,” Phys. Med. Biol. 58(20), p. 7419-7445, 2013

[14] J. S. Karp, S. Surti, M. E. Daube-Witherspoon and G. Muehllehner, “Benefit of time-of-flight in PET: experimental and clinical results,” J. Nucl. Med., 49(3), p. 462-470, 2008

[15] V. Y. Panin, F. Kehren, C. Michel and M. E. Casey “Fully 3-D PET reconstruction with system matrix derived from point source measurements,” IEEE Trans. in Med. Imag., 25(7), p. 907-921, 2006

[16] B. W. Jakoby, Y. Bercier, M. Conti, M. E. Casey, B. Bendriem and D. W. Townsend, “Physical and clinical performance of the mCT time-of-flight PET/CT scanner,” Phys Med Biol, 56(8), p. 2375-2389, 2011

[17] N. A. Karakatsanis, M. A. Lodge, A. Rahmim, and H. Zaidi, “Introducing Time-of-Flight and Resolution Recovery Image Reconstruction to Clinical Whole-body PET Parametric Imaging,” IEEE Nucl Sc Symp Med Imag Conf (NSS/MIC), Seattle, WA, 2014

[18] A. Rahmim, and J. Tang, “Noise propagation in resolution modeled PET imaging and its impact on detectability,” Phys Med Biol, 58(19), p. 6945-6968, 2013

[19] S. Ashrafinia, N. Karakatsanis, H. Mohy-ud-Din, and A. Rahmim, “Towards continualized task-based resolution modeling in PET imaging. Proc. SPIE Med Imag: Phys Med Imag, 903327, 2014

[20] S. Ashrafinia, H. Mohy-ud-Din, N. A. Karakatsanis, D. J. Kadrmas, and A. Rahmim, “Enhanced quantitative PET imaging utilizing adaptive partial resolution modeling,” J Nucl Med, 55 (suppl. 1), p. 371, 2014

[21] M Dahlbom, D C Yu, S R Cherry, A Chatziioannou and E J Hoffman, “Methods for improving image quality in whole body PET scanning.” IEEE Trans Nucl Sc, 39(4), p. 1079-1083, 1992

[22] S. R. Cherry, M. Dahlbom, and E.J. Hoffman, “High sensitivity, total body PET scanning using 3D data acquisition and reconstruction,” IEEE Trans Nucl Sci, 39(4), p. 1088-1092, 1992

[23] M. Dahlbom, A. Chatziioannou, and C. K. Hoh, "Resolution characterization of continuous axial sampling in whole body PET," IEEE Nucl Sc Symp Med Imag Conf (NSS/MIC), San Francisco, CA, 1995

[24] M. A. Flower, K. Erlandsson, P. Collins, A. J. Reader, J. R. Symonds-Tayler, L. L. White, and R. J. Ott, “Spiral whole-body PET - Implementation and initial results,” J Nucl Med, 40(5), p. 279, 1999

[25] K. Erlandsson, M. A. Flower, P. Collins, A. J. Reader, J. R. N. Symonds-Tayler, L. L. White, and R. J. Ott, R. "Spiral PET for whole-body studies with rotating planar detectors," Proc. Int. Meet Fully 3D Imag Recon Radiol Nucl Med, p. 77-79, 1999

[26] M. Dahlbom, J. Reed, and J. Young, "Implementation of true continuous bed motion in 2-D and 3-D whole-body PET scanning," IEEE Trans Nucl Sc, 48(4), p. 1465-1469, 2001

[27] D. Brasse, D. Newport, J. P. Carney, J. T. Yap, C. Reynolds, J. Reed, J. Bao, P. Luk, C. Michel, and D. W. Townsend, "Continuous bed motion acquisition on a whole body combined PET/CT system," IEEE Nucl Sc Symp Med Imag Conf (NSS/MIC), Norfolk, VA, 2, p. 951-955, 2002

[28] D. W. Townsend, J. Reed, D. F. Newport, J. PJ Carney, S. Tolbert, D. Newby, J. T. Yap, and M. J. Long, "Continuous bed motion acquisition for an LSO PET/CT scanner," IEEE Nucl Sc Symp Med Imag Conf (NSS/MIC), Rome, Italy, 4, p. 2383-2387, 2004

[29] Z. Burbar, C. Michel, D. Towsend, B. Jakoby, M. Sibomana, F. Kehren, S. Tolbert, J. Reed, K. Hubner, and M. Abidi, "Continuous bed motion data processing for a resolution LSO PET/CT scanner.," IEEE Nucl Sc Symp Med Imag Conf (NSS/MIC), Puerto Rico, 4, p. 2046-2048, 2005

[30] D. F. Newport, M. E. Casey, W. K. Luk, and J. H. Reed, "Continuous tomography bed motion data processing apparatus and method," U.S. Patent 6,915,004, July 5, 2005

[31] V. Y. Panin, "Random Sinogram Variance Reduction in Continuous Bed Motion Acquisition," U.S. Patent Application 13/737,437, January 9, 2013

[32] V. Y. Panin, and M. E. Casey, "Normalization Coefficients in PET Continuous Bed Motion Acquisition," U.S. Patent Application 13/739,458, January 11, 2013

[33] V. Y. Panin, A. M. Smith, and M. E. Casey. "Normalization coefficient computing for continuous bed motion acquisition," IEEE Nucl Sc Symp Med Imag Conf (NSS/MIC), Seoul, S. Korea, p. 1-10, 2013

[34] V. Y. Panin, A M Smith, J Hu, F. Kehren and M. E. Casey, "Continuous bed motion on clinical scanner: design, data correction, and reconstruction," Phys Med Biol, 59(20), p. 6153-6174, 2014

[35] D R Osborne, S Acuff, S. Cruise, M. Syed, M. Neveu, A. Stuckey and Y. Bradley "Quantitative and qualitative comparison of continuous bed motion and traditional step and shoot PET/CT," Am J Nucl Med Mol Imag, 5(1), p. 56-64, 2015

[36] I. Schatka, D. Weiberg, S. Reichelt, N. Owsianski-Hille, T. Derlin, G. Berding, and F. M. Bengel, "A randomized, double-blind, crossover comparison of novel continuous bed motion versus traditional bed position whole-body PET/CT imaging," Eur J Nucl Med Mol Imag, p. 1-7, 2015

[37] C. C. Watson, M. E. Casey, T. Beyer, T. Bruckbauer, D. W. Townsend, and D. Brasse "Evaluation of clinical PET count rate performance," IEEE Trans Nucl Sc, 50(5), p. 1379-1385, 2003

[38] T. Chang, G. Chang, S. Kohlmyer, J. W. Clark Jr, E. Rohren, and O. R. Mawlawi, "Effects of injected dose, BMI and scanner type on NECR and image noise in PET imaging," Phys Med Biol, 56(16), p. 5275-5285, 2011

[39] C. C. Watson, M. E. Casey, B. Bendriem, J. P. Carney, D. W. Townsend, S. Eberl, S. Meikle, and F. P. DiFilippo, "Optimizing injected dose in clinical PET by accurately modeling the counting-rate response functions specific to individual patient scans," J Nucl Med, 46(11), p. 1825-1834, 2005

[40] Y. Masuda, C. Kondo, Y. Matsuo, M. Uetani, and K. Kusakabe, "Comparison of imaging protocols for 18F-FDG PET/CT in overweight patients: optimizing scan duration versus administered dose," J Nucl Med, 50(6), p. 844-848, 2009

[41] T. Carlier, L. Ferrer, H. Necib, L. L. Meunier, F. Schoenahl, C. Bodet-Milin, C. Rousseau, and F. Kraeber-Bodéré, "Optimization of acquisition parameters for 18F-FDG PET scans using the clinical NECR." J Nucl Med, 54, (suppl. 2), p. 2088-2088, 2013

[42] T. Carlier, L. Ferrer, H. Necib, C. Bodet-Milin, C. Rousseau, and F. Kraeber-Bodéré, "Clinical NECR in 18F-FDG PET scans: optimization of injected activity and variable acquisition time. Relationship with SNR," Phys Med Biol, 59(21), p. 6417-6430, 2014

[43] N. A. Karakatsanis, G. Loudos, A. Rahmim, and K. S. Nikita, "Monte-Carlo based characterization of the counting rate (NECR) response for personalized optimization of the administered activity in clinical PET imaging," Front Biomed Tech, 1(1), p. 14-34, 2014

[44] N. A. Karakatsanis, E. Fokou, and C. Tsoumpas, "Dosage optimization in positron emission tomography: state-of-the-art methods and future prospects," Am J Nucl Med Mol Imag, 5(5), p. 527, 2015

[45] W. Zhu, Q. Li, and R. M. Leahy, "Dual-time-point Patlak estimation from list mode PET data," IEEE Int Symp Biom Imag (ISBI), p. 486-489, 2012

[46] N. A. Karakatsanis, M. A. Lodge, R. L. Wahl and A. Rahmim, "Direct 4D whole-body PET/CT parametric image reconstruction: concept and comparison vs. indirect parametric imaging," J Nucl Med, 54(Supplement 2), p. 2133-2133, 2013

[47] N. A. Karakatsanis and A. Rahmim, "Whole-body PET parametric imaging employing direct 4D nested reconstruction and a generalized non-linear Patlak model," Proc. SPIE Med Imag: Phys Med Imag, 90330Y, 2014

[48] W. Zhu, Q. Li, B. Bai, P. S. Conti, and R. M. Leahy, "Patlak image estimation from dual time-point list-mode PET data," IEEE Trans Med Imag 33(4), p. 913-924, 2014

[49] W. Zhu, N. Guo, B. Bai, P. S. Conti, R. M. Leahy, and Q. Li, "Direct estimation from list-mode data for reversible tracers using graphical modeling," IEEE Int Symp Biom Imag (ISBI), p. 1204-1207, 2015

[50] C. S. Patlak, R. G. Blasberg, and J. D. Fenstermacher, "Graphical evaluation of blood-to-brain transfer constants from multiple-time uptake data," J. Cereb. Blood Flow Metab., 3(1), p. 1-7, 1983

[51] C. S. Patlak and R. G. Blasberg, "Graphical evaluation of blood-to-brain transfer constants from multiple-time uptake data. Generalizations," J. Cereb. Blood Flow Metab., 5, p. 584-590, 1985

[52] N. A. Karakatsanis, Y. Zhou, M. A. Lodge, M. E. Casey, R. L. Wahl, H. Zaidi and A. Rahmim, "Quantitative whole-body parametric PET imaging incorporating a generalized Patlak model," IEEE Nucl Sc Symp Med Imag Conf (NSS/MIC), p. 1-9, 2013

[53] N. A. Karakatsanis, Y. Zhou, M. A. Lodge, M. E. Casey, R. L. Wahl, H. Zaidi and A. Rahmim "Generalized whole-body Patlak parametric imaging for enhanced quantification in clinical PET," Phys Med Biol, 60(22), p. 8643-8673, 2015

[54] N. A. Karakatsanis, M. A. Lodge, M. E. Casey, H. Zaidi and A. Rahmim, "Impact of Acquisition Time-Window on Clinical Whole-Body PET Parametric Imaging," IEEE Nucl Sc Symp Med Imag Conf (NSS/MIC), 2014

[55] N. A. Karakatsanis, M. Lodge, Y. Zhou, M. Casey, R. Wahl, R. Subramaniam, H. Zaidi, and A. Rahmim, "Novel multi-parametric SUV/Patlak FDG-PET whole-body imaging framework for routine application to clinical oncology," J Nucl Med, 56 (Supplement 3), p. 625-625, 2015

[56] Y. Zhou, S. Zhang, J. Zhang, N. Karakatsanis, A. Rahmim, M. Lodge, R. Wahl, D. Wong, and R. F. Wang, "Generalized population-based input function estimation given incomplete blood sampling in quantitative dynamic FDG PET studies," J Nucl Med, 53 (Supplement 1), p. 380-380, 2012

[57] N. Karakatsanis, Y. Zhou, M. Lodge, M. Casey, R. Wahl, R. Subramaniam, A. Rahmim, and H. Zaidi, "Clinical Whole-body PET Patlak imaging 60-90min post-injection employing a population-based input function," J Nucl Med 56, (Supplement 3), p. 1786-1786, 2015